V European Conference on Computational Fluid Dynamics
ECCOMAS CFD 2010
J. C. F. Pereira and A. Sequeira (Eds)
Lisbon, Portugal, 14–17 June 2010

THREE-DIMENSIONAL PORE SCALE FLUID FLOW SIMULATION BASED ON COMPUTED MICROTOMOGRAPHY CARBONATE ROCKS' IMAGES

Jan Kaczmarczyk[*†], Marek Dohnalik[†], Jadwiga Zalewska[†]

[†]Oil and Gas Institute
Well Logging Department
ul. Bagrowa 1
30-733 Kraków, Poland
e-mail: jan.kaczmarczyk@inig.pl

Key words: computed microtomography, permeability, fluid flow, geophysics, reservoir rocks parameters

Abstract. *Internal rock's structure based on X-ray computed microtomography (CMT) measurement may be used to fluid flow simulation and evaluating of rock's reservoir properties.*

CMT makes it possible to see real pores' shapes and connections between the pores in rock samples. That's why simulation based on CMT data is particularly interesting. Reconstructed structure of pore network allows use of the Navier-Stokes equations to simulate fluid flow through the pores, so the fluid flow is simulated without any experimental data (like it is when Darcy's law is used) about rock's porosity and permeability. Moreover, the calculations based on CMT data may lead to estimate permeability of reservoir rocks' samples without the use of chemical reagents.

After structure reconstruction sample's image was prepared to simulation by segmentation (phase-mean thresholding), pores' extraction, filtering and resampling. The fluid flow was simulated in COMSOL Multiphysics 3.5a Earth Science module. Used fluids were nitrogen, propane, water, gasoline and engine oil (fluid parameters were taken from COMSOL material library). Temperature was set to 298 K and external pressure was set to 1013 hPa. The inlet parameter was pressure. The outlet was defined as open boundary without viscous stress. The steady state fluid flow was simulated.

Simulations were performed on 8-core PC (2.66 GHz per each core) with 32 GB RAM. Each simulation took about 0.5 hour.

Simulations showed significant differences between fluids velocities in pore networks. The maximal velocities were decreasing in order: propane, gasoline, water, engine oil. The higher viscosity of fluid the lower maximal it's velocity in rock's pore network. Nevertheless, relative changes of velocities are the same in case of all examined fluids. Calculated permeability values were consistent with results of gas-permeability experiment.

1 INTRODUCTION

1.1 Reservoir rocks' parameters

The main task of geophysics in oil industry is to tell where the oil deposits are present. The presence of hydrocarbons deposits is determined on the basis of rocks' examination. Basic reservoir rocks' parameters, examined during laboratory test, are porosity and permeability.

Porosity is defined as a volume of sample occupied with the gases (air, hydrocarbons) or liquids (water, hydrocarbons). This property defines how much hydrocarbons may be pumped from the examined rocks. Porosity is measured with the use of absorption measurements.

Permeability is material's ability to allow fluid flow through it. It defines how difficult the hydrocarbons pumping will be. It is evaluated with the use of Darcy's law[1]:

$$K = -\frac{\eta \cdot u_D}{\nabla p}, \tag{1}$$

in gas permeability test equipment – the difference of pressure between fluid's inlet and outlet is measured. In equation 1 K is the permeability, η is the fluid viscosity, u_d is Darcy's velocity and p the pressure.

The good reservoir rock should be characterized by high porosity and high permeability.

1.2 Navier-Stokes equations

The Navier-Stokes equations are the fundamental equations of fluid flow. The most general form of these equations is[2, 3]:

$$p\frac{d\boldsymbol{u}}{dt} + (p\boldsymbol{u}\cdot\nabla)\boldsymbol{u} = -\nabla p + \nabla\cdot\left(\eta(\nabla\boldsymbol{u} + (\nabla\boldsymbol{u})^T)\right) + \boldsymbol{F}, \tag{2}$$

$$\nabla\cdot\boldsymbol{u} = 0, \tag{3}$$

where p is the pressure, $\boldsymbol{u}$ is a fluid velocity, t is time, η is the fluid dynamic viscosity and $\boldsymbol{F}$ is the external force field (vector sizes were bolded). First equation is the mass conservation equation and the second one is the continuity equation.

For the pore-space fluid flow, where the capillary forces dominate, the **F** = 0. Also, the permeability test mentioned in paragraph 1.1 is conducted after nitrogen flow stabilization, so to simulate this measurement steady-state may be assumed and the equation 2 becomes time-independent. Thus, the equation 2 may be simplified to form:

$$(p\boldsymbol{u}\cdot\nabla)\boldsymbol{u} = -\nabla p + \nabla\cdot\left(\eta(\nabla\boldsymbol{u} + (\nabla\boldsymbol{u})^T)\right). \tag{4}$$

Permeability of material may be calculated on the basis of Navier-Stokes equations with the use of formula[2]:

$$K = \frac{\frac{\varepsilon}{A}\cdot L_i\cdot\int_A u_i dA}{\frac{\nabla p}{\gamma}}, \tag{5}$$

where ε is sample's porosity L_i – the length of the sample in i direction, u_i - the fluid velocity in i direction, A – area of fluid outlet in given direction, ∇p – the gradient of pressure and γ– the fluid unit weight calculated as:

$$\gamma = \rho\cdot g, \tag{6}$$

where ρ is the fluid density and g = 9.81 m·s^{-2} is the acceleration due to the gravity.

1.3 Computed microtomography in geophysics

Computed microtomography (micro-CT, CMT) is rather new research method in geophysics. It is based on Radon's principles of computed tomography. During the computed microtomography measurement the examined object is rotating and the X-ray projections of examined object at various angles are recorded. Gray value of each pixel on the projection is defined with the Beer's law for complex materials[4]. Next, during the reconstruction process, the internal structure of examined object is calculated as the superposition of recorded projections. The resolution is typical in order of micrometers. With the use of submicro- or nano-CT system, images with resolution down to 50 nm may be obtained[5].

The result of reconstruction is a volume image (gray scale point cloud) where the gray level of each voxel (volume picture element) is proportional to the attenuation coefficient of object's volume element (which is proportional to material's density and atomic number of elements occurring in this volume element)[6].

Reconstructed image, after the use of proper binarization method, may be used for porosity calculation. Tomographic porosity is calculated as:

$$\varepsilon = \frac{V_p}{\sum_i V_i}, \tag{7}$$

where V_p is a volume of pores' layer and V_i is the volume of *i*-layer. Porosity calculated on the basis of CMT image is lower than porosity estimated with the use of adsorption methods. This is due to the image resolution – on tomographic rock's image it is impossible to see pores with a volume less than reconstruction resolution.

The data obtained with the computed microtomography measurements may be also used to estimate permeability of examined rock with the use of equation 6 after the fluid flow simulation. Applicability of equation 5 was confirmed during the experiment made on porous material model[2].

2 OBJECTIVES

The first objective of this paper was to show authors' methodology of preparing image obtained with the use of CMT method to FEM fluid flow simulation. The second objective was to calculate rock's permeability on a basis of fluid flow simulation results and compare it with permeability estimated during gas permeability test. Third objective was to examine flow of different fluids through the rock's pore network.

3 EXPERIMENTAL

Finite element method calculations were made on the basis of microtomographic carbonate rocks' images. This section provides detailed description of experiment, image processing and calculations settings.

3.1 Samples

Three carbonate rocks (from drilling areas in Poland) were examined. The samples were cut in the form of cylindrical core with diameter of 10 mm (figure 1).

Samples of carbonate rocks with regular apertures were selected. This was due to the easier image processing in case of aperture's image.

3.2 CMT equipment

Measurements were performed on X-Tek Benchtop CT160Xi apparatus. The current on X-ray source (with tungsten filament) was about 50 μA and the voltage was 110 kV. The Varian PaxScan 2520V flat panel detector with pixel area 127×127 μm^2 was used.

The exposure time was 0.5 s (2 frames per second). During the measurement about 3000 projections were made (one projection per every angle). The measurement took about 3 hours. Experimental system is shown on figure 1.

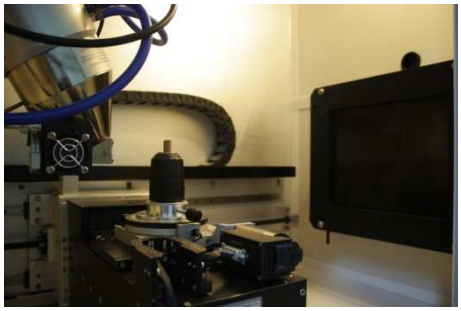

Figure 1: Experimental X-Tek Benchtop CT160Xi system; on the left: X-ray gun with tungsten reflection target, sample's holder and manipulator with examined rock core, flat panel detector.

3.3 Computer hardware

All operations were performed on Dell workstations. Computer for reconstruction and image processing was Intel Xeon X5355 2.66 GHz with 16 GB RAM and Windows XP x64 operating system. FEM fluid flow simulations were run on Intel Xeon E5430 2.66 GHz with 32 GB RAM and Windows Vista 64-bit operating system.

3.4 Reconstruction

Structure of each sample was reconstructed with the use of X-Tek CT-Pro software[7]. Center of rotation was found with accuracy 0.1 px (pixel). All recorded X-ray projections were used in reconstruction process. Region of interest (ROI) was about 1700×1700×700 voxels. The reconstruction resolution was 6.0×6.0×6.0 μm^3.

3.5 Binarization and surface generation

Image processing was made in VSG Avizo 6.1[8]. Reconstructed images were cropped to a cuboid to avoid participation of surrounding air in porosity. Images were binarized with the use of phase-mean thresholding method[9].

Number of density phases (density phase is a phase that has attenuation coefficient significantly different than its' surrounding; after binarization every phase is marked as another layer) were estimated on the image visually. Next, the average (based on 10 voxels) gray level of each phase was calculated. The threshold values were calculated as the average of averages for two phases with similar gray values.

After binarization the 25 % of 3D islands with volume up to 15 voxels were removed. Than porosity was calculated according to equation 7 and binarized image was saved as an 8-bit raw file.

Surfaces were generated in Simpleware's ScanIP[10]. The binarized raw image was imported and the pores, which made connection between image's opposite sides, were selected with the use of FloodFill segmentation tool (every pore was assigned to another layer. Image was downsampled by factor 5 (sample 1), 3 (sample 2) and 10 (sample 3). Layers were resampled with the use of partial volume effect resampling and background was linearly resampled. Then, to prevent pore network's rupture during resampling, the dilatation morphological filter (based on a ball with diameter of 1 voxel) was used. Surfaces of selected pores were generated and saved as STL files without smoothing. The steps of geometric model generation are shown on figures 2-4.

(a) (b)

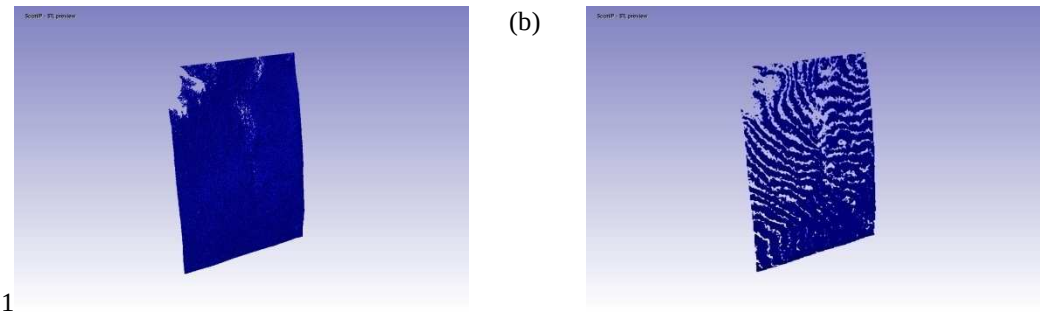

1

(c)

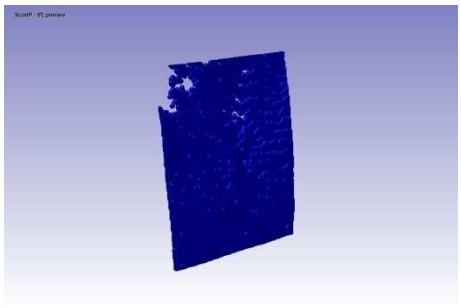

Figure 2: Preparation of geometrical model of sample 1 (original size: 440×539×672 voxels): (a) basic image, (b) surface downsampled by factor 5, (c) downsampled surface after application of morphological filter; the pores' extracting was not necessary.

(a) (b)

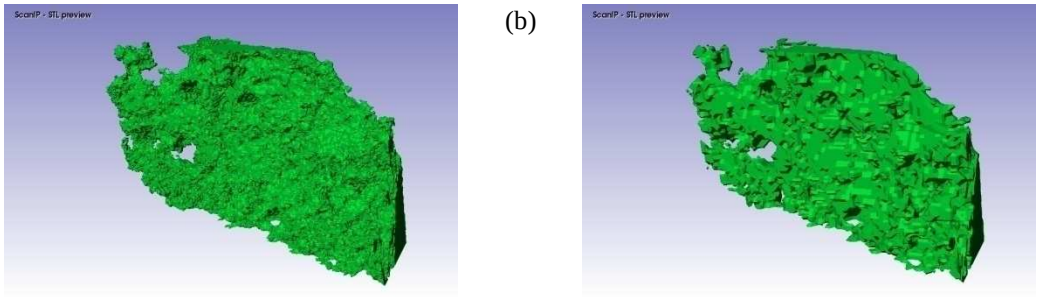

(c)

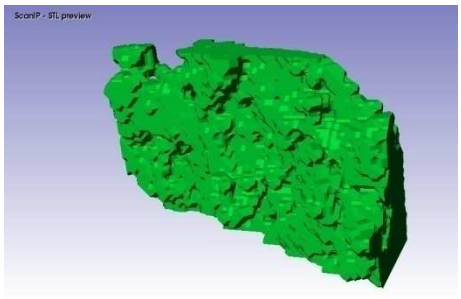

Figure 3: : Preparation of geometrical model of sample 2 (original size: 233×278×132 voxels): (a) basic image, (b) surface downsampled by factor 3, (c) downsampled surface after application of morphological filter; the pores' extracting was not necessary.

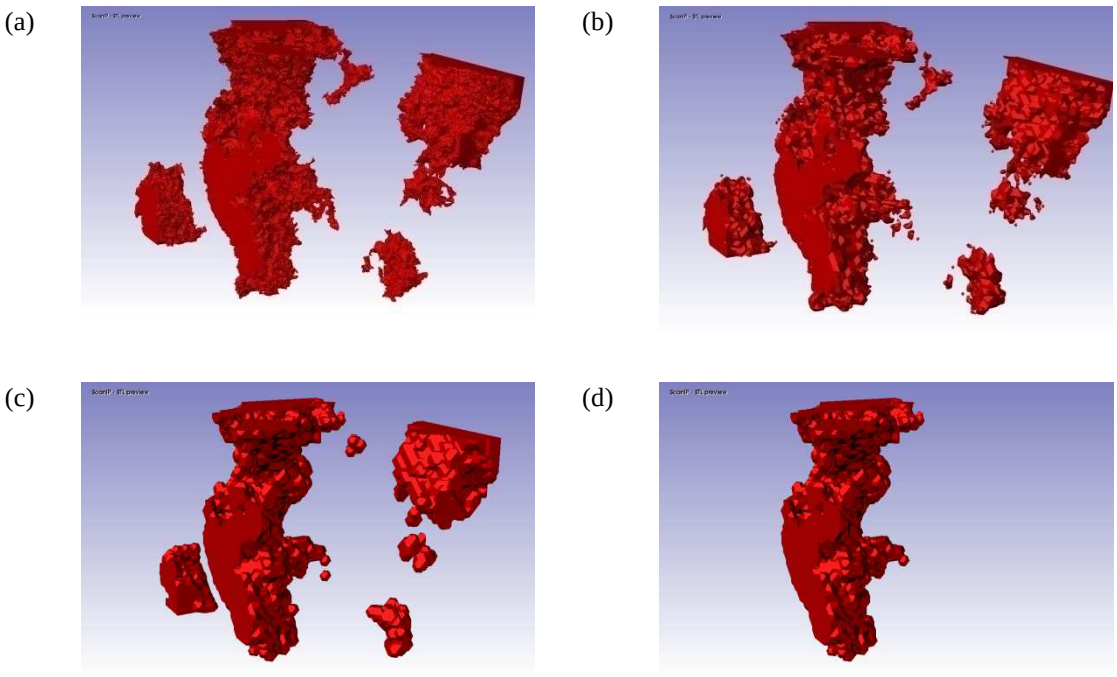

Figure 4: Preparation of geometrical model of sample 3 (original size: 880×560×606 voxels): (a) basic image, (b) surface downsampled by factor 10, (c) downsampled surface after application of morphological filter, (d) pore's extraction.

4 FLUID FLOW SIMULATION

Fluid flow was simulated in COMSOL Multiphysics 3.5a Earth Science Module[11] in incompressible Navier-Stokes mode. Detailed description of calculation settings is available in software documentation[3, 12, 13].

4.1 Model definition

Surface, generated in previous step, was imported. As the global constants temperature T (T = 298 K) and pressure p_0 (p_0 = 1,013·10^5 Pa) were defined. The surface's subdomain was filled with certain fluid: propane, water, gasoline, engine oil or nitrogen. Fluids characteristics were taken from COMSOL Material Library and are shown in table 1. Subdomain stabilization techniques (for geometric multigrid with Lagrange P_1P_2 elements) were used: GLS, streamline diffusion (0.1) and crosswind diffusion (0.1). The improved residual approximation for linear elements was selected.

fluid	ρ /kg·cm^{-3}	η /Pa·s	γ /kg·s^{-2}·m^{-2}
nitrogen	1.20	1.76·10^{-5}	11.80
propane	18.71	0,81·10^{-5}	183.52
gasoline	746.08	50·10^{-5}	7319.04
water	998.25	89·10^{-5}	9792.80
engine oil	884.70	0.55	8678.92

Table 1: Properties (for T = 298 K and p_0 = 1013·10^5 Pa) of fluids used in fluid flow simulations, taken from COMSOL Multiphysics 3.5a Material Library[11].

Inputs and outputs were placed on the opposite sides of the sample in z direction (rotation axis during the CMT measurement). The input was defined with the input pressure ($1{,}05 \cdot p_0$). Output was defined as the open boundary without vicious stress. The mesh was created with the use of COMSOL meshing module (mesh quality was defined as “fine”).

4.2 Solver parameters

Steady-state PARADISO (Direct) solver was used. Relative tolerance was set to $5 \cdot 10^{-5}$. Stationary solver was set for 100 iterations and tolerance $5 \cdot 10^{-5}$. Using of complex functions with real input was allowed.

5 RESULTS

5.1 Simulations results

The number of mesh elements, degrees of freedom (DOF) and average computation time for every sample is shown in table 2.

Sample	number of mesh elements	DOF	computation time /s
1	179440	918600	630
2	227680	1080300	1600
3	281700	1347500	2230

Table 2: Average number of mesh elements, degrees of freedom (DOF) and computation times for each sample.

As it was shown in table 2, calculations in case of samples 2 and 3 took about 30 minutes. For sample 1 they took about 10 minutes. This is due to the simplest geometry of crack in sample 1.

On figures 5-7 the results of all simulations are shown.

(a)

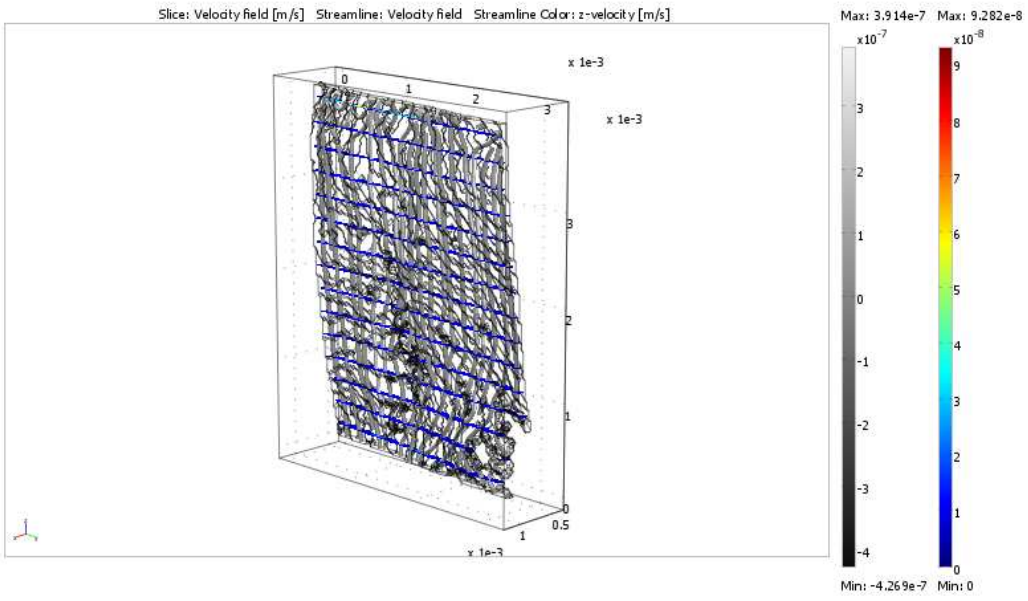

(b)

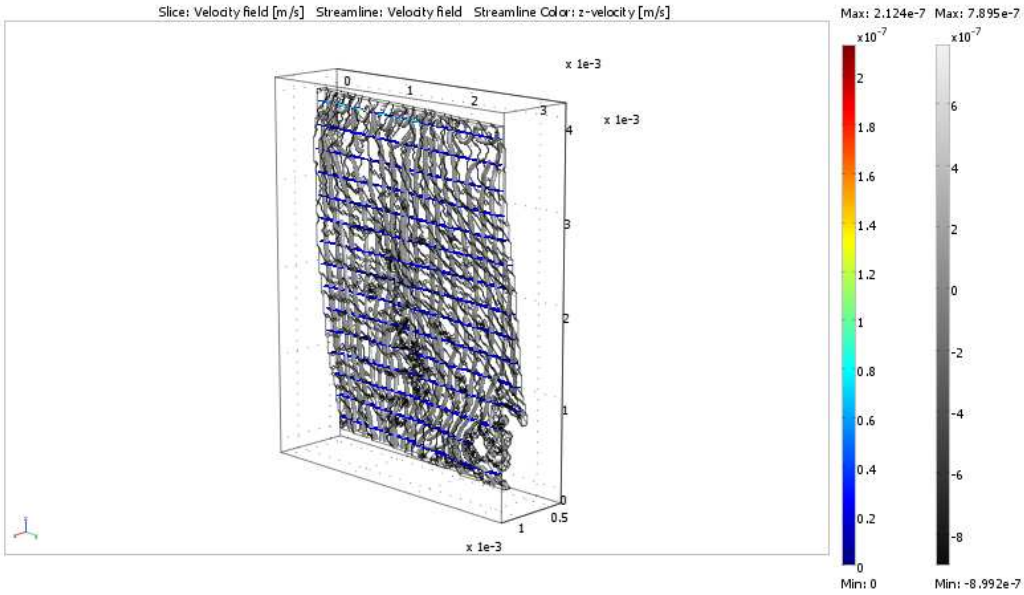
Slice: Velocity field [m/s] Streamline: Velocity field Streamline Color: z-velocity [m/s]
x 1e-3
x 1e-3
x 1e-3
Max: 2.124e-7
Min: 0
Max: 7.895e-7
Min: -8.992e-7

(c)

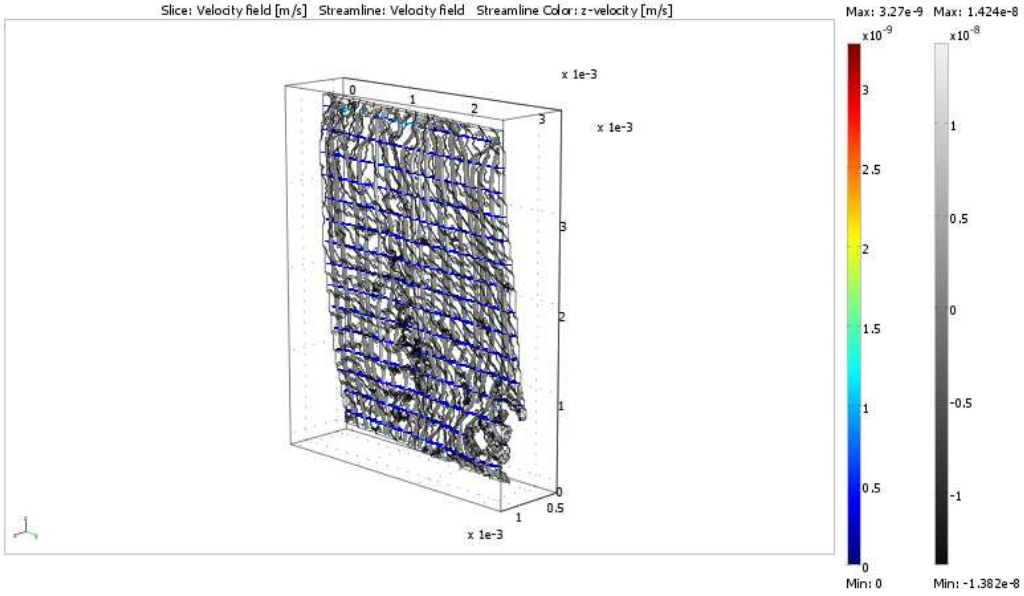
Slice: Velocity field [m/s] Streamline: Velocity field Streamline Color: z-velocity [m/s]
x 1e-3
x 1e-3
x 1e-3
Max: 3.27e-9
Min: 0
Max: 1.424e-8
Min: -1.382e-8

(d)

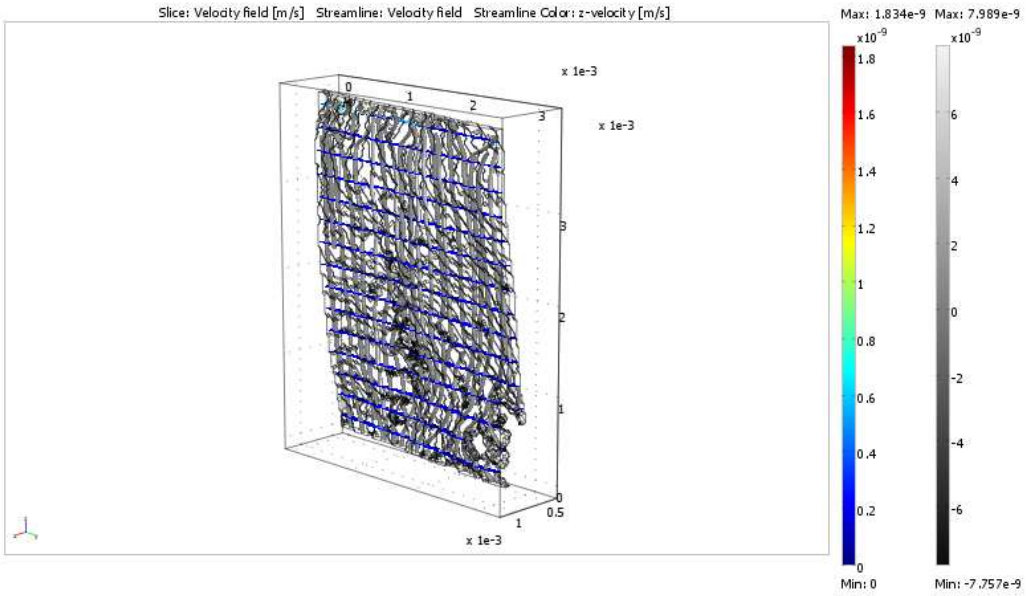

(e)

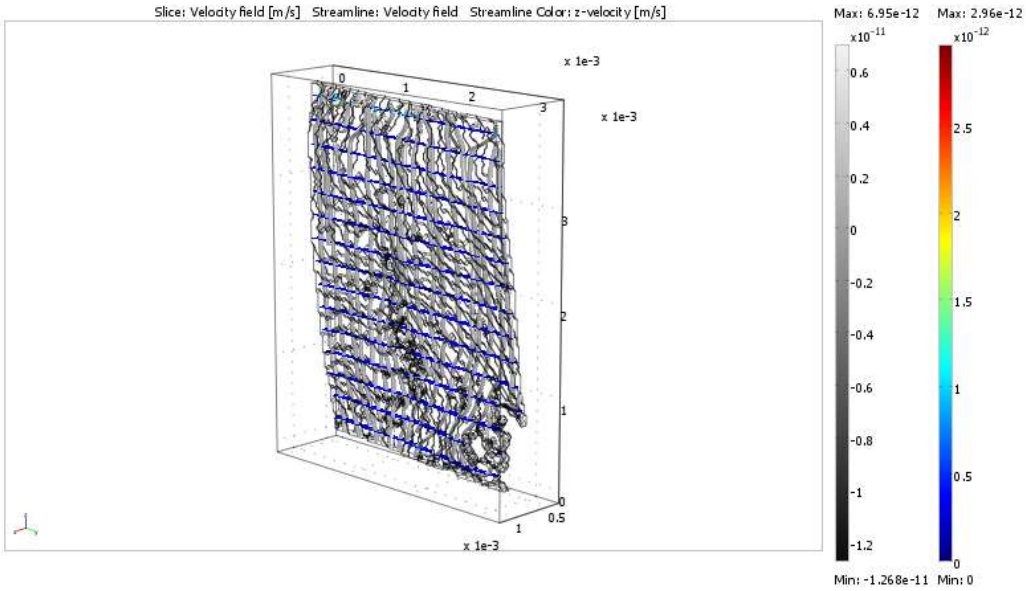

Figure 5: Simulations' results for sample 1: (a) nitrogen, (b) propane, (c) gasoline, (d) water, (e) engine oil; the tubes shows the velocity field lines, tube's color – velocity z-component value, slices – velocity field value;

(a)

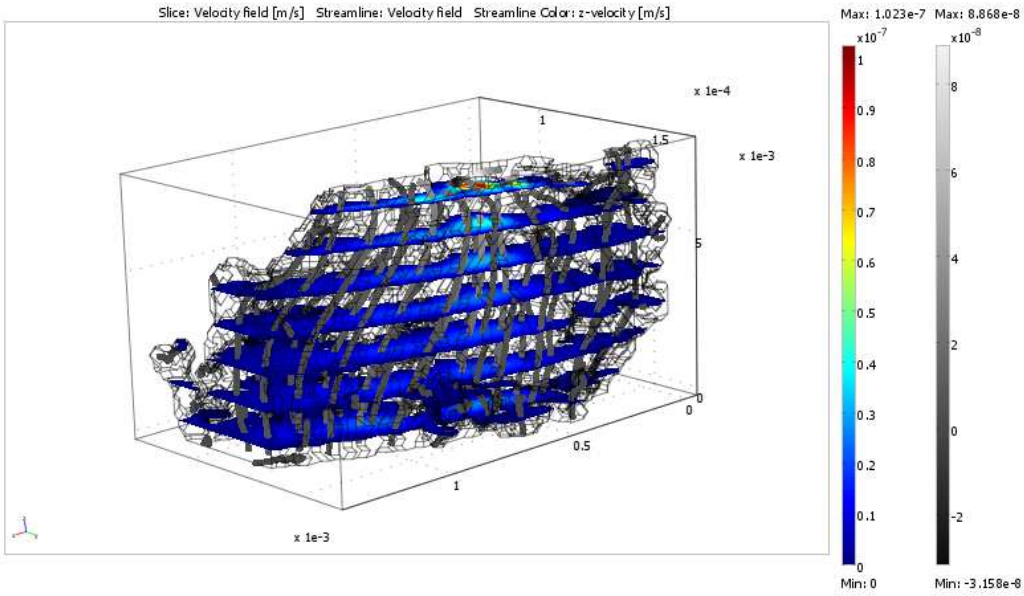
Slice: Velocity field [m/s] Streamline: Velocity field Streamline Color: z-velocity [m/s]
x 1e-4
x 1e-3
x 1e-3
Max: 1.023e-7
Max: 8.868e-8
Min: 0
Min: -3.158e-8

(b)

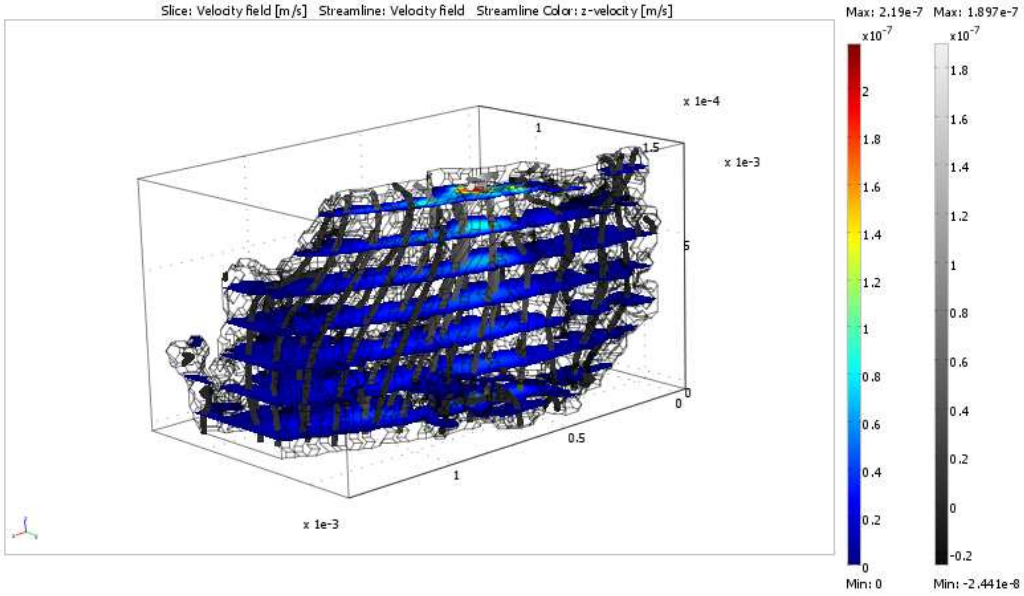
Slice: Velocity field [m/s] Streamline: Velocity field Streamline Color: z-velocity [m/s]
x 1e-4
x 1e-3
x 1e-3
Max: 2.19e-7
Max: 1.897e-7
Min: 0
Min: -2.441e-8

(c)

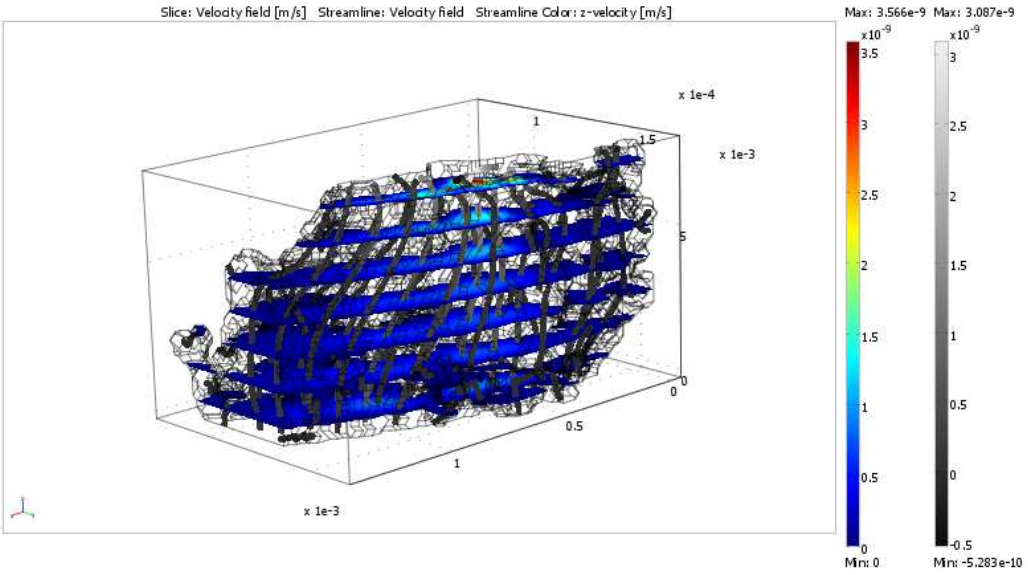
Slice: Velocity field [m/s] Streamline: Velocity field Streamline Color: z-velocity [m/s]
x 1e-4
x 1e-3
x 1e-3
Max: 3.566e-9
Min: 0
Max: 3.087e-9
Min: -5.283e-10

(d)

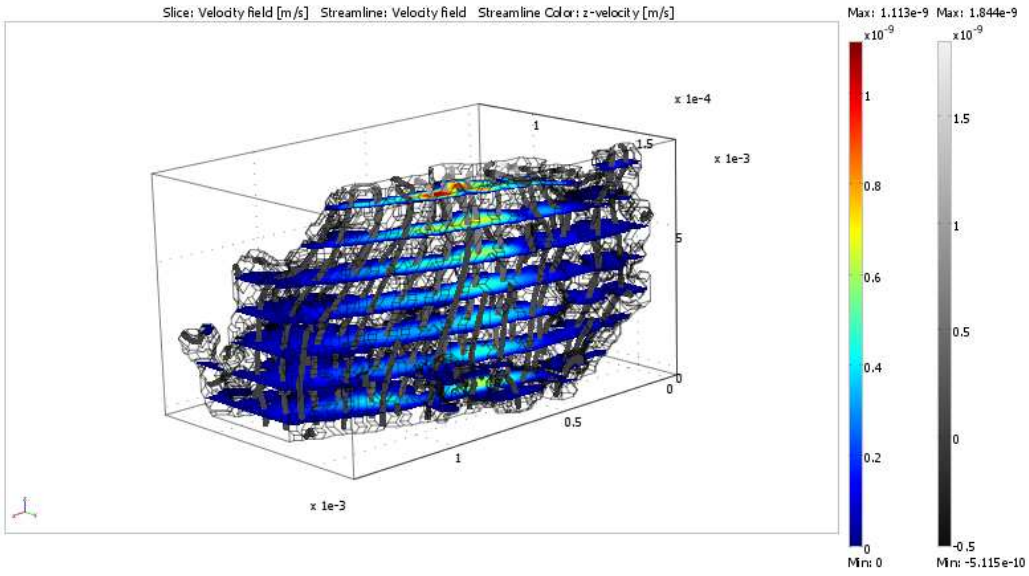
Slice: Velocity field [m/s] Streamline: Velocity field Streamline Color: z-velocity [m/s]
x 1e-4
x 1e-3
x 1e-3
Max: 1.113e-9
Min: 0
Max: 1.844e-9
Min: -5.115e-10

(e)

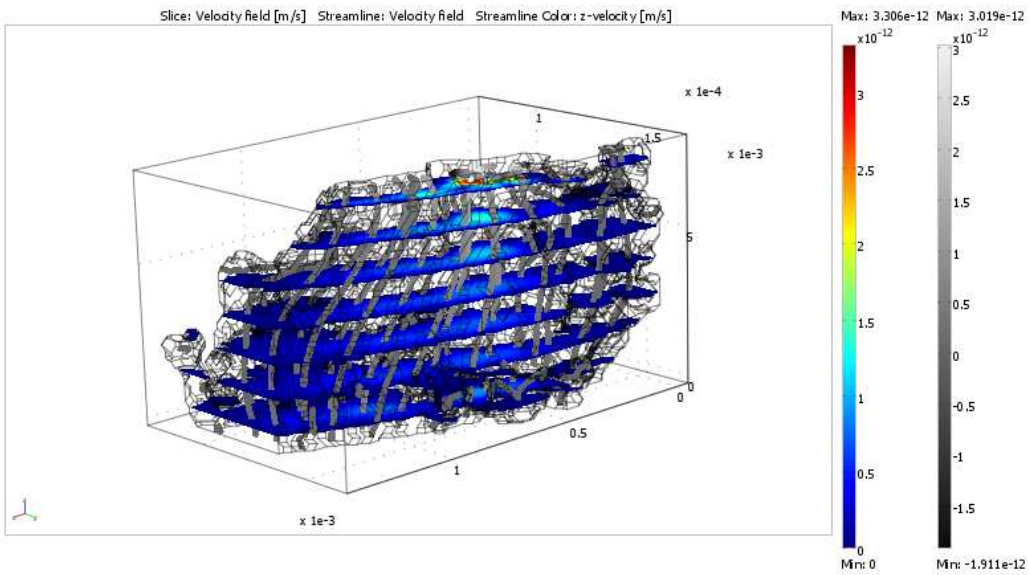

Figure 6: Simulations' results for sample 2: (a) nitrogen, (b) propane, (c) gasoline, (d) water, (e) engine oil; the tubes shows the velocity field lines, tube's color – velocity z-component value, slices – velocity field value;

(a)

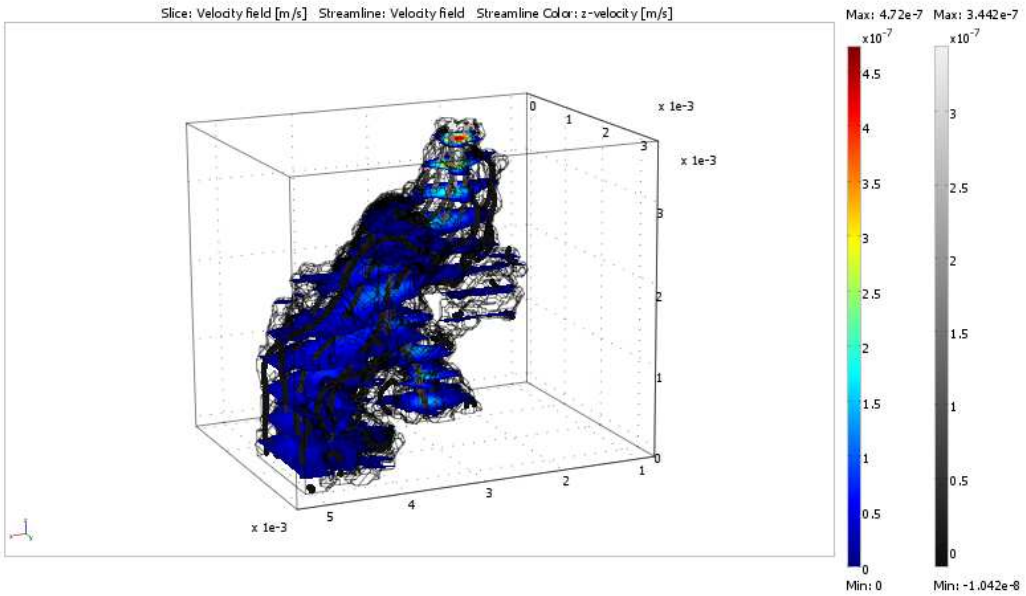

(b)

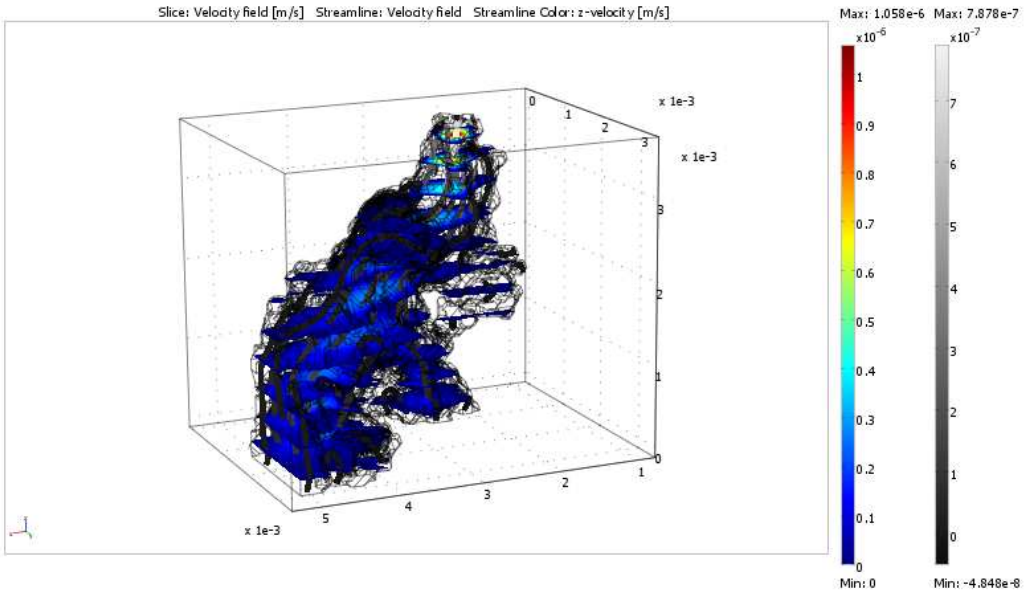
Slice: Velocity field [m/s] Streamline: Velocity field Streamline Color: z-velocity [m/s]
Max: 1.058e-6
Max: 7.878e-7
Min: 0
Min: -4.848e-8
x 1e-3
x 1e-3
x 1e-3

(c)

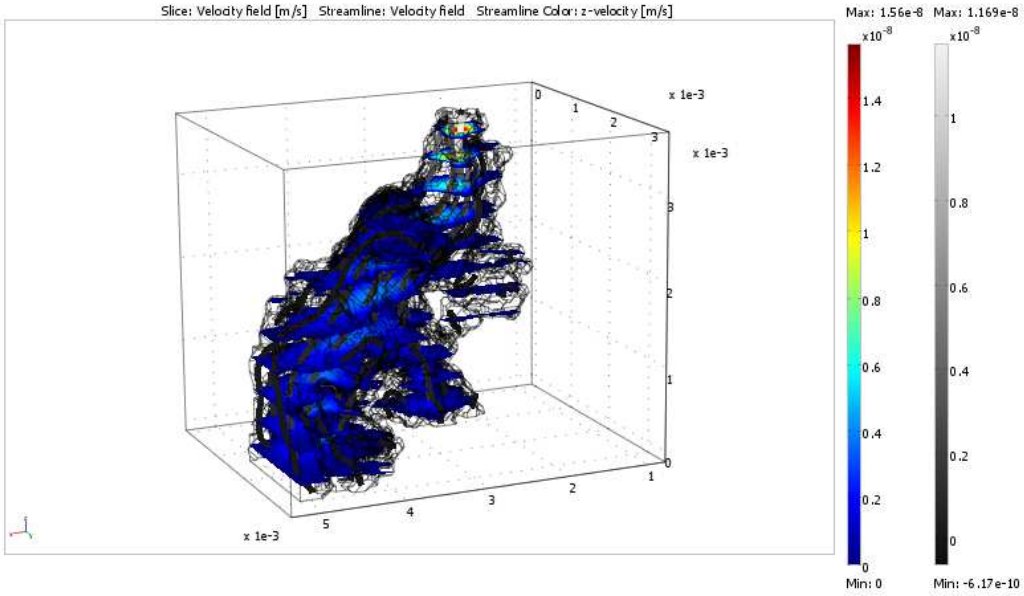
Slice: Velocity field [m/s] Streamline: Velocity field Streamline Color: z-velocity [m/s]
Max: 1.56e-8
Max: 1.169e-8
Min: 0
Min: -6.17e-10
x 1e-3
x 1e-3
x 1e-3

(d)

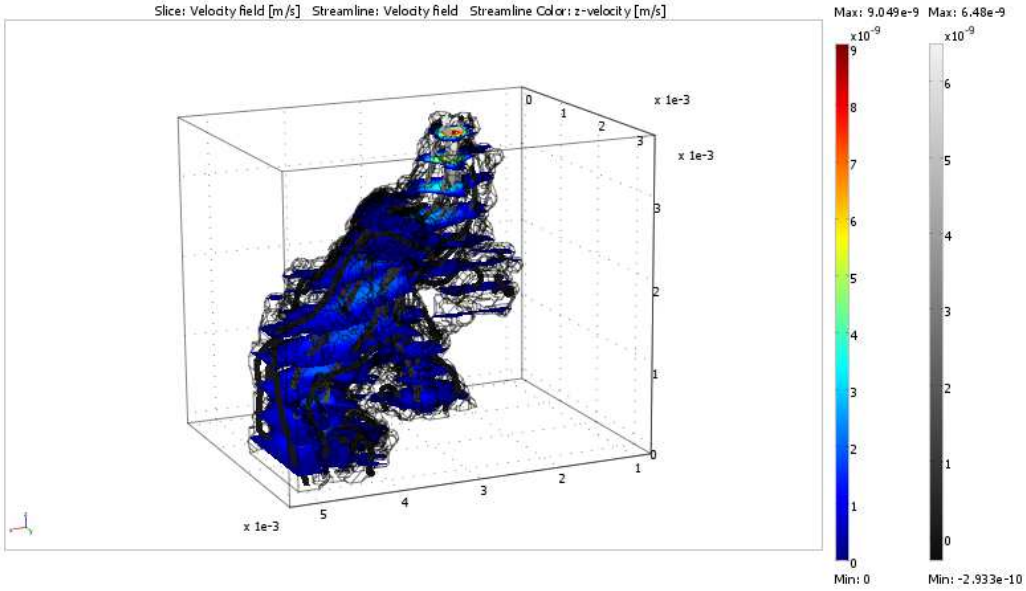

(e)

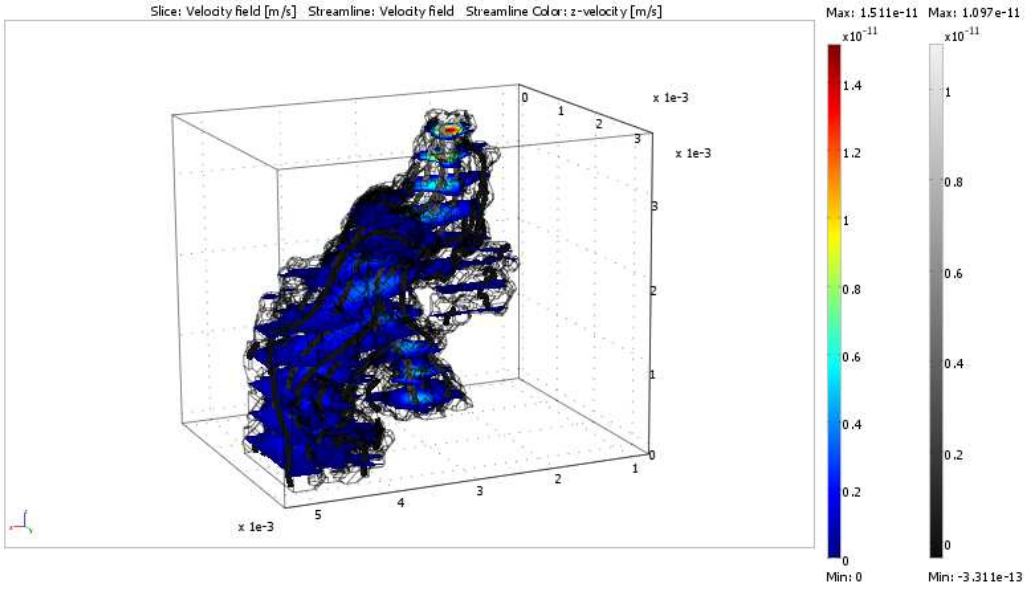

Figure 7: Simulations' results for sample 3: (a) nitrogen, (b) propane, (c) gasoline, (d) water, (e) engine oil; the tubes shows the velocity field lines, tube's color – velocity z-component value, slices – velocity field value;

5.2 Permeability calculations

Permeability was calculated with the use of equation 5 in simplified form:

$$k_{N-S} = \frac{\frac{\varepsilon}{A} L_z \cdot \int_A w dA}{\frac{\Delta p}{\gamma}}, \tag{8}$$

where the L_i was replaced with L_z (the length of model in z-direction, based on the number of voxels in original image), the ∇p with Δp (the difference of the pressures between top and bottom of the sample) and u_i with w (velocity z-component). The CMT properties of examined rocks' and their geometrical models are shown in table 3.

sample	L /10^{-3}m	ε /%	A /10^{-7}m^3
1	4.032	1.1	3.2
2	0.792	10.3	1.3
3	3.646	15.3	3.1

Table 3: Examined rocks' properties evaluated with the use of CMT method.

The permeability calculation results are shown in table 4.

sample	Δp /10^{-7}Pa	$\int_A wdA$ /10^{-15}m^{3}s^{-1}	$k_{N\text{-}S}$ /mD	K_{exp} /mD
1	30.9	2.2	0.07	0,09
2	6.6	2.1	36.43	37,34
3	4.9	63.0	212.58	0,10

Table 4: Results of nitrogen flow simulation; K_{exp} is the permeability value measured during the gas permeability test.

With the assumption that measured permeability is an accurate value, the absolute error may be calculated as:

$$\Delta K = \left|k_{N-S} - K_{exp}\right|. \tag{9}$$

Also, the relative error may be calculated with the use of expression:

$$\Delta k = \frac{\left|k_{N-S} - K_{exp}\right|}{K_{exp}} \cdot 100\%. \tag{10}$$

Results of errors estimation are shown in table 5.

sample	ΔK /mD	Δk /%
1	0.02	22.2
2	0.94	2.5
3	19.29	203900.0

Table 5: Absolute and relative errors values for permeability calculations.

As it was shown in tables 4 and 5, in case of samples 1 and 2 calculated and measured permeability values were similar. This shows applicability of chosen methodology for rocks' permeability calculations. In case of sample 3 the real and calculated permeability were totally different. However, sample 3 was the only one downsampled by factor 10, so generated surface was the most distorted (in comparison with original image).

For samples 1 and 2 calculated permeability was lower that experimental value. This is due to the used microtomography system resolution. In performed experiment pores with dimensions below 6 μm couldn't be seen. In fact, these pores may provide other fluid flow ways through the rock and increase permeability.

5.3 Reservoir fluids flow simulations

Despite the fact that permeability value calculated for sample 3 is incorrect, calculation results for this sample may be used to qualitative analysis of fluid behavior in pore space. Results for the two other samples may be used to qualitative fluid behavior's analysis.

In table 6 the maximum velocities (total and z-component) of fluids in case of each sample are compared.

sample	fluid	u_{max} /m·s^{-1}	w_{max} /m·s^{-1}
1	propane	$1.2 \cdot 10^{-5}$	$1.9 \cdot 10^{-6}$
	gasoline	$1.9 \cdot 10^{-7}$	$3.0 \cdot 10^{-8}$
	water	$1.1 \cdot 10^{-7}$	$1.7 \cdot 10^{-8}$
	engine oil	$1.9 \cdot 10^{-10}$	$2.8 \cdot 10^{-11}$
2	propane	$1.5 \cdot 10^{-6}$	$3.0 \cdot 10^{-7}$
	gasoline	$2.4 \cdot 10^{-8}$	$4.8 \cdot 10^{-9}$
	water	$1.2 \cdot 10^{-8}$	$2.7 \cdot 10^{-9}$
	engine oil	$2.6 \cdot 10^{-11}$	$3.8 \cdot 10^{-12}$
3	propane	$3.5 \cdot 10^{-6}$	$1.1 \cdot 10^{-6}$
	gasoline	$5.6 \cdot 10^{-8}$	$1.7 \cdot 10^{-8}$
	water	$1.4 \cdot 10^{-8}$	$1.1 \cdot 10^{-8}$
	engine oil	$2.2 \cdot 10^{-11}$	$1.9 \cdot 10^{-11}$

Table 6: Maximum fluids' velocities for each sample.

It may be noticed that maximum fluid velocity and its z-component was proportional to fluid's viscosity. This is consistent with physical intuition. In case of each sample, the maximum velocity for propane was about 10^5 times higher than maximum velocity for engine oil (in case of total velocity and its z-component).

The velocities attained in sample 1 were about 10 times higher than in sample 2. This is due to the crack's geometry. Crack in sample 1 is quite simple – it has a shape of slightly inclined plane – so the fluid may flow along the straight lines. In sample 2 crack has more undulating surface and there's several places where fluid flow may be inhibited.

As it was shown in figures 5-7. the relative changes in fluid's velocities are the same in case of each examined fluid. This is also correct – in given pore space different fluids have to flow in the same way and the different viscosity causes differences in fluid velocity.

6 CONCLUSIONS

Studies shown, that used methodology of model preparatix1on is proper for CMT-based fluid flow simulation. The most important step in model preparation in the downsampling. The higher downsampling factor is the faster simulation is. On the other hand – the downsampling may deform pores' shapes and if the downsampling factor is too high, the simulation will give wrong permeability value.

Performed simulations shown that maximum velocities reached by fluid particles in pore space are viscosity dependent. The higher viscosity is the lower velocity is. The differences in velocity between examined fluids were in order of 10^5. Relative changes in fluid's velocities during the flow through the pore space were the same in case of every fluid.

The utility of computed microtomography method for reservoir rocks' examination was demonstrated. Thus, this method may be useful for oil industry applications. It's safer than currently being used gas permeability test, because it does not require use of any chemical agent.

7 SUMMARY

Results of FEM fluid flow simulations (based on Navier-Stokes equations) for three carbonate rocks samples were shown. In case of two of them, calculated permeability

values were close to the values obtained with the use of gas permeability test. The results for third sample were distracted because of the model preparation process – the pore space shape was deformed in the downsampling step.

The application of computed microtomography for reservoir rocks' parameters calculation was shown. The CMT method provides a safe method for permeability and porosity evaluation.

8 ACKNOWLEDGEMENTS

This paper includes results obtained during realizing statutory research DK-4100-26/10 funded by Republic of Poland Ministry of Science and Higher Education.

9 REFERENCES

[1] E. Zaman, J. Payman, On hydraulic permeability of random packs of monodisperse spheres: Direct flow simulations versus correlations, Physica A **389**, iss. 2, pp. 205-214 (2010)

[2] G. Narsilio, O. Buzzi, S. Fityus, T. Yun, D. Smith, Upscaling of Navier–Stokes equations in porous media: Theoretical, numerical and experimental approach, Comput. Geotech. **36**, iss. 7, pp. 1200-1206 (2009)

[3] COMSOL Multiphysics 3.5a Modeling Guide, COMSOL AP (2008)

[4] R. Ketcham, W. Carlson, Acquisition, optimization and interpretation of X-ray computed tomographic imaginery: applications to the geosciences, Comput. Geosci. 27, iss. 4, pp. 381-400 (2001)

[5] J. Izzo Jr., A. Joshi, K. Grew, W. Chiu, A. Tkachuk, S. Wang and W. Yun, Nondestructive Reconstruction and Analysis of SOFC Anodes Using X-ray Computed Tomography at Sub-50 nm Resolution, J. Electrochem. Soc. **155** (5), pp. B504-B508 (2008)

[6] V. Cnudde, B. Masschaele, M. Dietrick, J. Vlassenbroeck, L. Van Hoorebeke, P. Jacobs, Recent progress in X-ray CT as a geosciences tool, Appl. Geochem. 21, iss. 5, pp. 826-832 (2006)

[7] X-Tek CT-Pro, http://www.xtekxray.com/products/computed_tomography.html

[8] VSG Avizo 6.1, http://www.vsg3d.com/vsg_prod_avizo_overview.php

[9] J. Kaczmarczyk, M. Dohnalik, J. Zalewska, V. Cnudde, The interpretation of X-ray Computed Microtomography images of rocks as an application of volume image processing and analysis, WSCG2010 Communication Paper Proceedings, pp. 23-30 (2010)

[10] Simpleware's ScanIP 3.2, http://www.simpleware.com/software/scanip.php

[11] COMSOL Multiphysics 3.5a, http://www.comsol.com/

[12] COMSOL Multiphysics 3.5a User's Guide, COMSOL AP (2008)

[13] COMSOL Multiphysics 3.5a Earth Science Module User's Guide, COMSOL AP (2008)